Sensors & Transducers, Vol. 186, Issue 3, March 2015, pp. 118-124

Sensors & Transducers

http://www.sensorsportal.com

Synthesis of Cu Doped ZnO Nanostructures for Ultra Violet Sensing

[*1] Nazar Abbas SHAH, [2] Muhammad ABID, [3] Muhammad AMIN, [3] Rahat AFRIN and [2] Syed Zafar ILYAS

[1] Thin Films Technology Laboratory, Department of Physics, COMSATS Institute of Information Technology, Islamabad 44000, Pakistan

[*] Tel.: +92-03215105363,

[2] Department of physics, Allama Iqbal Open University Islamabad, Pakistan

Tel.: 92-306-8883730

[3]DESTO Lab, Islamabad 44000, Pakistan

E-mail: abid742197@yahoo.com, aminislamabad@yahoo.com, rahin_6@yahoo.com, nabbasqureshi@yahoo.com

Received: 17 December 2014 /Accepted: 27 February 2015 /Published: 31 March 2015

Abstract: This paper mainly focused on the synthesis of zinc oxide nanostructures, their characterization and their ultra violet light sensing response at room temperature. Nanowires, nanobelts and nanosheets were synthesized by varying doping material copper by using vapor transport technique governed by the vapor-liquid-solid or vapor-solid mechanisms. The structural, morphological and optical characterization was carried out using X-ray diffraction, scanning electron microscopy, energy dispersive X-Ray and ultra violet visible spectroscopy techniques. Finally the ultra violet light sensing response of these nanostructures was observed by using Keithley meter. The high ultra violet photosensitivity and fast response time justifies the effective utilization of these ZnO nanostructures as ultra violet sensors in different areas. *Copyright © 2015 IFSA Publishing, S. L.*

Keywords: ZnO nanostructures, Vapor-liquid-solid method, UV sensor, Optical properties.

1. Introduction

Among various metal oxide semiconducting materials, zinc oxide (ZnO) is a distinctive electronic and photonic wurtzite n-type semiconductor with a wide direct band gap of 3.37 eV, high exciton binding energy (60 meV) at room temperature, and strong piezoelectric and optical properties. The high exciton binding energy of ZnO would allow for excitonic transitions even at room temperature. Oxides are the basis of various smart and functional materials [1]. Device fabrication using oxide semiconductors has gained significant importance, because physical properties of these oxides can be tuned. ZnO nanostructures can be synthesized by numerous synthesis methods such as electrochemical, vapor phase, and liquid phase techniques [2–6]. The vapor transport method is one of the most extensively explored due to single crystal structure and high aspect ratio of the resulting nanostructures. The growth kinetics of ZnO nanostructures by the vapor liquid solid (VLS) method depends on many factors i.e., activation energy of crystallization, radius of catalyst droplets, super-saturation, synthesis temperature, volume of liquid droplets, and the equilibrium vapor pressure of the system. The

thermodynamic limit for the critical radius of the metal liquid cluster at high temperature is given by Equation (1) [6]:

$$Rmin = 2\, r_{LV}\, \alpha / KT \ln S, \quad (1)$$

where r_{LV} is the liquid vapor surface free energy, α is the molar volume of liquid and S is the vapor phase super-saturation. The above relation suggests that there is a critical limit on the diameter and the ratio of super saturation whereas temperature has direct effect on the growth of 1-D structures. In recent years, there has been considerable interest in developing reliable UV sensors. ZnO based sensors have gained particular importance due to several advantages such as wide operating temperature range, flexibility in processing to thin/thick film during device fabrication, high sensitivity to UV radiation, carrier mobility, and good chemical and thermal stability [7]. Recently it was reported that response time of ZnO based sensors strongly depends on the size, specific surface area and morphology [8]. The sensing mechanism of ZnO is linked with surface-controlled reactions in which grain size, defects, and oxygen adsorption play a crucial role in the sensing response [9]. In the present study, systematic control of different ZnO nanostructure morphologies and their optical and UV sensing properties are presented. ZnO nanowires, nanobelts and nanosheets were synthesized by varying doping material (copper nitrate) by using vapor transport technique governed by the vapor-liquid-solid (VLS) mechanism. The synthesis of ZnO nanobelts and nanosheet by varying quantity of dopping material (copper nitrate) at constant furnace temperature 1020 ^{o}C governed by VLS mechanism is unique as to our knowledge. These ZnO nanostructures are promising materials for low-cost and high-performance UV sensors at room temperature. The results show good response to UV radiations of 360nm at room temperature.

2. Experimental Section

Experimental work consists of a series of three experiments. In this work ZnO nanowires, nanobelts and nanosheets were synthesized by VLS method. Source materials, zinc oxide (99.9 %) and graphite in powder form, were mixed in 1:1 weight ratio for 2 hr in a planetary ball mill (Fritsch, Pulverisette 5). Copper nitrate $Cu(NO_3)_2.3H_2O$ was used for doping of copper in experiment # 2&3. About 1 g of this mixture was transferred to an Al_2O_3 boat. Gold coated Si substrates were placed on top of the boat for the deposition of ZnO nanostructures. The boat was placed in the center of a quartz tube (diameter= 3.5 cm and length=100 cm). This quartz tube was then placed inside a tube furnace which was ramped to the required temperature 1020 °C @ 10 °C/min. Argon was used as the carrier gas, while growth time (Dwell time) fixed at 1 hour and Ar flow rate was fixed at 50 SCCm, in all the experiments. The other end of quartz tube was attached to a flexible tube (diameter 1.0 cm and length 100 cm) and was kept open.

X-Ray diffraction (XRD), scanning electron microscopy (SEM) and energy dispersive X-Ray (EDX) were used to determine the crystal structure, morphology and element analysis of the grown nanostructures. Band gap energy was calculated by using UV-visible absorbance spectroscopy. The UV sensors were fabricated by depositing 50 nm thick gold electrodes onto quartz substrates through sputter deposition technique and the respective ZnO nanostructures were placed between electrodes (through doctor blading). The response of the device was measured by observing the resistance behavior upon exposure of the device to UV radiation at room temperature. A multimeter (Keithly 2000) was used to measure the respective resistance values. The UV sensing response in the form of resistance change was observed as shown in Fig. 1.

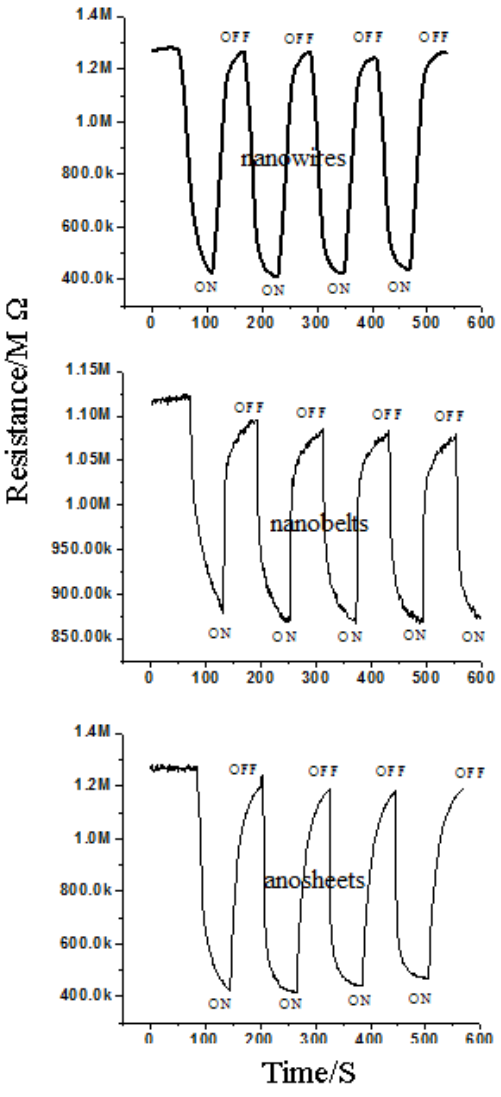

Fig. 1. UV sensing results of different morphologies of ZnO Nanostructures: (a) Undoped ZnO Nanowires; (b) Cu doped ZnO Nanobelts; (c) Cu doped ZnO Nanosheets.

3. Results and Discussion

3.1. Scanning Electron Microscopy

SEM micrographs of ZnO nanostructures synthesized in series of three experiments are shown in Fig. 2(a-c). Fig. 2 (a) shows SEM images of undoped ZnO nanowirs. These were synthesized by source material without doping of copper. The general morphology of the samples consists of a net of nanowires. The length of these wires was found to be in tens of microns range and the average diameter of 60.2 nm ± 7.7 nm. The possible reason for growth of such nanowires is that the wurtzite structure of ZnO exhibits polar-terminated (0001) and non polar low-symmetry (10$\underline{1}$0) faces. It is well-known that in most situations the growth rates of the different family of planes follow the sequence (0001) > (10$\underline{1}$1) > (10$\underline{1}$0) [12, 26, 31]. There are several reasons why the (0001) plane shows the highest growth speed, promoting the one-dimensional growth. One is that the Zn (0001) plane has the lowest surface energy, which tends to be the most stable to resist oxidation [28]. Since the temperature of the growth zone is above the Zn melting temperature, this liquid-phase growth front is highly effective to absorb the incoming Zn vapor and maintains high growth speed. Another factor is that the top areas of nanowires always receive a high flux of Zn vapor than the shaft due to the shadow effect intrinsic to all physical vapor processes [27]. If the growth along the [0001] direction dominates, then nanowires grow continuously with homogeneous diameters [29].

Fig. 2(b) shows SEM image of Cu doped ZnO nanobelts. Nanobelts synthesized by doping of copper 3.5 % in ZnO (By adding suitable quantity of $Cu(NO_3)_2.3H_2O$ in source material). These belts have average width and thickness of 1.15 μm ± 0.08 μm and 77.3 nm ± 9 nm, respectively. Fig 1(c) is the SEM image of Cu doped ZnO nanosheets. Nanosheets synthesized by doping of copper 7% in ZnO. These sheets have average width (from centre) and thickness of 1.24 μm ± 0.23 μm and 53.55 nm ± 9.15 nm, respectively. All the SEM micrographs clearly suggest formation of nanostructures of different morphology at the same synthesis temperatures 1020 °C and experimental environment. Experimental results show that morphology of structures is changed due to doping of copper. The possible reason for this type of growth is attributed to higher super saturation, surface instability and quick availability of ZnO polar surfaces, since at higher super saturation; the atoms are readily available to these polar surfaces for random growth [5]. The possible reason of growth of nanobelts and nanosheets can be linked to a self-catalyzed process and morphological instability in a supersaturated environment [11]. One of the possible reasons for the growth of nanobelts and nanosheets is that rates of crystal growth in different directions in ZnO are different [12, 26, 31] and due to this difference, the crystal growth face takes a specific shape [29]. Overall, at different percentage of doping material, the supersaturating conditions are different which ultimately changes the morphology.

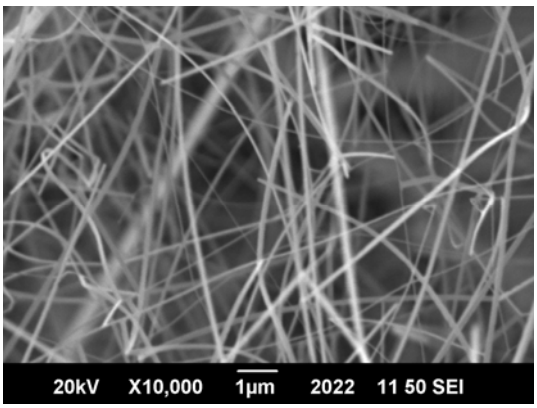

(a)

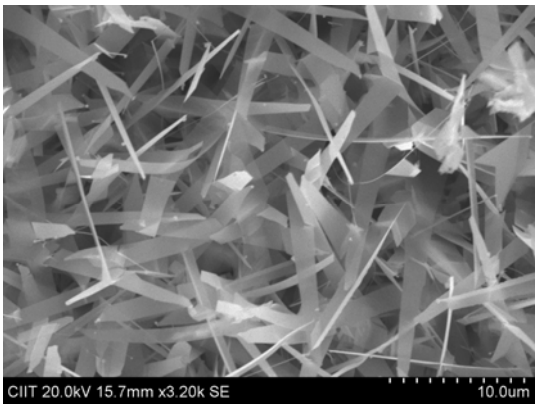

(b)

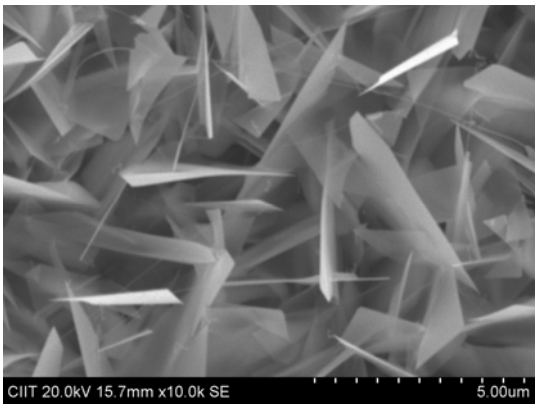

(c)

Fig. 2. SEM images of different morphologies of ZnO Nanostructures: (a) Undoped ZnO Nanowires; (b) Cu doped ZnO Nanobelts; (c) Cu doped ZnO Nanosheets.

3.2 Energy Dispersion X-Ray

EDX spectroscopy was then used to provide elemental analysis and study the compositions of the

synthesized nanostructures, with the obtained spectrum displayed in Fig. 3. In addition to Zn peaks at 1.03, 8.7 and 9.6 keV, an oxygen peak at 0.54 keV was observed. No peak of Cu was observed due to lower doping concentration of copper [30].

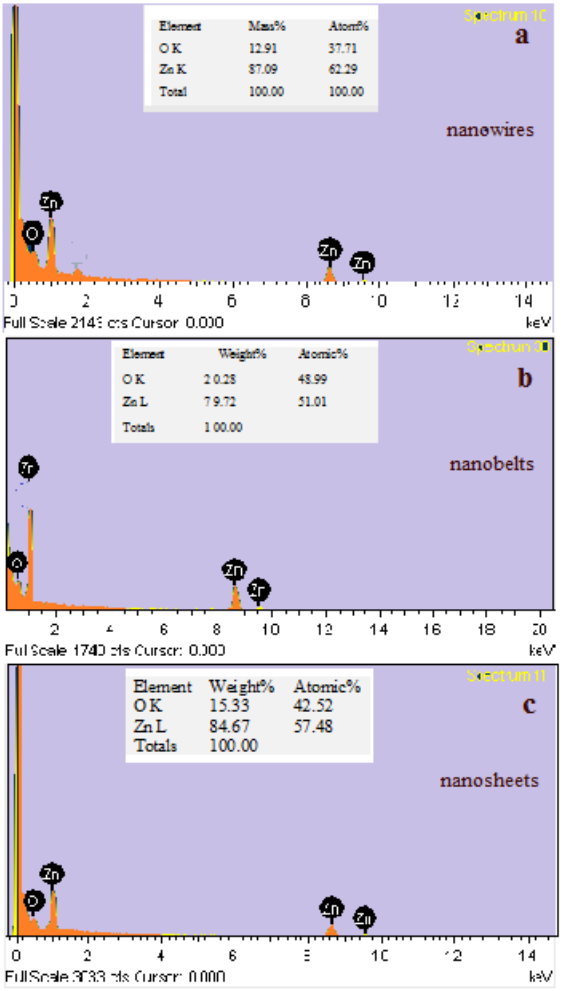

Fig. 3. EDX images of different morphologies of ZnO Nanostructures: (a) Undoped ZnO Nanowires; (b) Cu doped ZnO Nanobelts; (c) Cu doped ZnO Nanosheets.

3.3. X-Ray Diffraction

Analysis of the crystal structures of the synthesized ZnO nanostructures was performed with X-ray diffraction. XRD spectrums of synthesized ZnO nanostructures are shown in Fig. 4 (a-c). Fig 4 shows that the prominent peaks for undoped nanowires were observed at angles of 31.698º, 34.403º, 36.212º, 47.493º, 56.544º. The prominent peaks for Cu doped nanobelts were observed at angles of 31.712º, 34.387º, 36.212º, 47.497º, 56.531º and prominent peaks for Cu doped nanosheets were observed at angles of 31.694º, 34.429º, 36.196º, 47.483º, 56.525º. These peaks belong to the (100), (002), (101), (102), (110), planes respectively which confirm the formation of hexagonal wurtzite ZnO nanostructures.

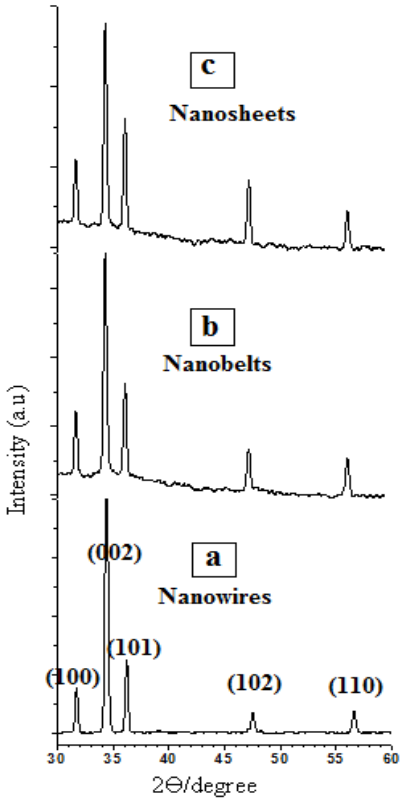

Fig. 4. XRD result of different morphologies of ZnO Nanostructures: (a) Undoped ZnO Nanowires; (b) Cu doped ZnO Nanobelts; (c) Cu doped ZnO Nanosheets.

No peaks that may correspond to impurities were detected, thus implying that a relatively high purity of ZnO nanostructures was obtained. EDX spectroscopy results also confirm the purity of ZnO nanostructures. X-ray diffraction results show that there is no significant peak shift. The minor peak shifting is due to replacement of Zn^{2+} ions with Cu^{2+} ions in small extent [29, 30]. The narrower FWHM suggests better crystalinity. The narrow FWHM may be due to higher synthesis temperatures (1020 ºC) [31] which help to enhance the mobility of atoms, subsequently resulting in reduced defect concentration and improved quality of the ZnO crystals [2, 9]. Sharp and relatively high intensity peaks were observed which depicts high crystalinity of synthesized nanostructures [31]. A strong (002) peak implies a c-axis preferred orientation in the synthesized nanostructures. Measured lattice parameters for synthesized nanostructures are given in Table 1. These parameters are comparable to the published values for the hexagonal wurtzite structure.

Table 1. Lattice parameters of nanostructures.

Morphology of nanostructures	a (Aº)	b(Aº)	c(Aº)
Nanowires	3.2596	3.2596	5.2138
Nanobelts	3.2582	3.2582	5.2161
Nanosheets	3.2600	3.2600	5.2100

3.4 Ultra Violet-Visible Spectroscopy

Room temperature UV-VIS absorption spectra of synthesized samples, after Kubelka-Munk treatment, are shown in Fig. 5. The optical gap was estimated from absorbance spectra by plotting the square of the Kubelka-Munk function $F(R)^2$ given by the relation

$$F(R) = (1-R)^2/2R,$$

where R is the absorbance as a function of energy. Fig. 5 shows the $F(R)^2$ as a function of energy for synthesized ZnO samples and to obtain the optical gap the linear part of $F(R)^2$ curve was extrapolated until it intersects the energy axis at $F(R)^2 = 0$. The optical band gap of the various ZnO samples is shown in Table 2. For undoped ZnO nanowires the band gap comes out to be 3.36 eV and is in accordance with the reported value [30]. For Cu-doped ZnO nanobelts and nanosheets the optical gap was obtained as 3.35 and 3.34 eV respectively. The band gap is found to decrease with increase Cu concentration in ZnO. Similar mitigation of the band gap with increasing Cu concentration has been reported earlier [32, 33]. The inherent reason for red shift in band edge in transition metal doped ZnO samples is due to the change of the sp-d exchange interaction between the band electrons and the localized d-electron of the Cu^{2+} ions [34].

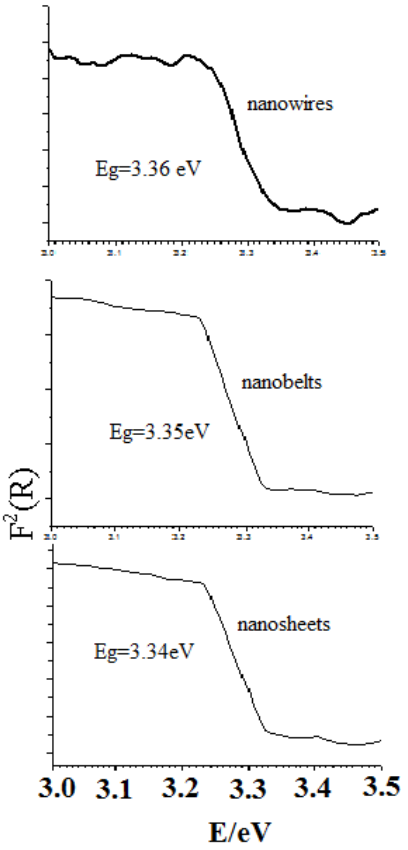

Fig. 5. Absorption spectroscopy results after Kubelka-Munk treatment of (a) Undoped ZnO Nanowires; (b) Cu doped ZnO Nanobelts; (c) Cu doped ZnO Nanosheets.

The UV slope is the exciton recombination related near-band edge emission (NBE) of ZnO and the deep-level emission (DLE) usually results from radiative recombination of a photo-generated hole with an electron occupying the oxygen vacancy [13]. With increase in synthesis temperature; there is a systematic increase in peak intensity, steeper slope of the absorption peak and a clear shift in the peak towards lower wavelengths was observed [31]. There are many reasons for different peak intensities, i.e., dispersed light due to scattering, electronic transitions in the samples, and variation in sample quantities. As it was not fixed, different nanostructure samples have different as-grown density on the substrate. However, increases in the intensity, steeper slopes, and shift in the slope with increase in the synthesis temperatures can be attributed to the improved quality of the crystal [31]. Two different groups in independent studies concluded that after high temperature treatment, UV peak intensity increases significantly, indicating that quality of ZnO is improved through annealing [4, 14]. Therefore, it can be deduced that high temperature synthesis plays an important role in tuning optical properties, and above-mentioned observations can be linked to the crystal quality of synthesized ZnO nanostructures. The calculated band gap values for all the structures are comparable to the theoretical value for ZnO.

XRD and UV-VIS spectroscopy results are in perfect agreement with each other. Steeper slopes, and increased UV and XRD intensities suggest decreases in the crystal defects and improved quality of the ZnO crystalline structure. Hence, it can be suggested that high synthesis temperatures provide energy to ZnO atoms for enhance mobility and diffusion that could decrease defect density and improve the quality of ZnO nanostructures [31].

3.5. UV Sensing

Fig. 1 shows the room temperature UV sensing results of ZnO nanostructures. The resistance decreases with exposure of UV light (wavelength ranges from 300 nm to 367 nm with 18 W UV Lamp, Phillips) and increases again when the UV lamp is switched off Photoconduction property of ZnO nanostructures enables them for Ultra Violet light sensors. As the band gap energy of the ZnO lies in the range of ultra violet region so when the ZnO nanostructures are exposed by the ultraviolet light, electrons transition takes place from the valence band to the conduction band it give rise to a current flow and decrease in the resistance [31].

When ZnO nanostructures are exposed to air, the negative space charge layer is created and the adsorbed oxygen molecule captures an electron from the conduction band (sensor exhibits higher resistivity). When the energy of photon is greater than the energy band gap Eg, radiation is absorbed by the ZnO nanostructures based UV sensor, creating an electron-hole pair. The photo-generated, positively-

charged hole neutralizes the chemisorbed oxygen (responsible for the higher resistance) increasing the conductivity of the device. As a consequence the conductivity in the material increases giving rise to photocurrent [31]. This process goes on in a cyclic manner with the on-off switching of the UV light. Sensing experiment shows that synthesized nanostructures have quick response to the UV light. As measured value of band gap energy for synthesized nanostructures is very close to actual value of ZnO (3.37 eV) hence maximum UV light activate the adsorption and desorption surface reactions with negligible losses. The reason of high sensitivity response and recovery time of synthesized nanostructures may be the crystallanity, and attributed to nanosize and dimensionality of the structures [9, 24]. XRD peaks also strengthen this statement. From the Fig. 1 it is observed that the response time was fast and recovery time was slow for nanobelts and nanosheets. The possible reason is that the different morphologies have different responses to the UV radiation; as different crystallographic directions or atomic termination of the faces that are exposed to the radiations are different [4]. The UV sensing response for synthesized nanostructures is given in Table 2.

Table 2. Summary of the results.

Morphology of nanostructures	Cu doping (%)	Bandgap (eV)	UV sensing response
Nanowires	0 %	3.36	3.25
Nanobelts	3.5 %	3.35	1.26
nanosheets	7 %	3.34	3.00

4. Conclusions

ZnO nanowires and copper doped nanobelts and nanosheets were successfully synthesized by using vapor transport technique. The structural, morphological and optical characterization was carried out using X-ray diffraction, scanning electron microscopy, and energy dispersive X-Ray and UV-visible spectroscopy techniques. XRD and optical properties suggest good crystallinity with low defect concentrations. Experimental results show that the band gap is found to decrease with increase Cu concentration in ZnO and morphology also changes due to Cu doping. Finally the UV light sensing response of these nanostructures was observed by using Keithley meter. The high UV photosensitivity and fast response time, justifies the effective utilization of these ZnO nanostructures as UV sensors in different areas.

Acknowledgments

The authors would like to thank Higher Education Commission (HEC) Pakistan. All the experimental work was done at COMSAT Institute of Information Technology, Islamabad. Thanks to CIIT for providing funding through project No. 16-27/CRGP/CIIT/IBD/13/225.

References

[1]. Z. R. Dai, Z. W. Pan, Z. L. Wang, Novel Nanostructures of functional oxides synthesized by thermal evaporation, *Advanced Functional Materials,* Vol. 13, 2003, pp. 9–24.

[2]. M. H. Wong, A. Berenov, X. Qi, M. J. Kappers, Z. H. Barber, B. Illy, Z. Lockman, M. P. Ryan, MacManus-Driscoll, J. L. Electrochemical growth of ZnO nano-rods on polycrystalline Zn foil, *Nanotechnology*, Vol. 14, 2003, pp. 968–973.

[3]. H. Hu, X. Huang, C. Deng, X. Chen, Y. Qian, Hydrothermal synthesis of ZnO nanowires and nanobelts on a large scale, *Materials Chemistry and Physics,* Vol. 106, 2007, pp. 58–62.

[4]. E. Comini, C. Baratto, G. Faglia, M. Ferroni, A. Vomiero, G. Sberveglieri, Quasi-one dimensional metal oxide semiconductors: Preparation, characterization and application as chemical sensors. *Progress in Materials Science,* Vol. 54, 2009, pp. 1–67.

[5]. S. Polarz, A. Roy, M. Lehmann, M. Driess, F. E. Kruis, A. Hoffmann, P. Zimmer, Structure-property-function relationships in nanoscale oxide sensors: A case study based on Zinc oxide, *Advanced Functional Materials,* Vol. 17, 2007, pp. 1385–1391.

[6]. D. Valerini, A. Creti, A. P. Caricato, M. Lomascolo, R. Rella, M. Martino, Optical gas sensing through nanostructured ZnO films with different morphologies, *Sensors and Actuators B,* Vol. 145, 2010, pp. 167–173.

[7]. T. Gao, T. H. Wang, Synthesis and properties of multipod-shaped ZnO nanorods for gas-sensor applications. *Applied Physics A,* Vol. 80, 2005, pp. 1451–1454.

[8]. J. H. Park, Y. J. Choi, J. G. Park, Synthesis of ZnO nanowires and nanosheets by an O2-assisted carbothermal Sreduction process. *J. Crystal Growth,* Vol. 280, 2005, pp. 161–167.

[9]. U. Manzoor, D. K. Kim, Size control of ZnO nanostructures formed in different temperature zones by varying Ar flow rate with tunable optical properties, *Physica E,* Vol. 41, 2009, pp. 500–505.

[10]. Z. L. Wang, X. Y. Kong, J. M. Zuo, induced growth of asymmetric nanocantilever arrays on polar surfaces, *Physical Review Letters,* Vol. 91, 2003, pp. 185502.

[11]. W. J. Li, E. W. Shi, W. Z. Zhong, Z. W. Yin, Growth mechanism and growth habit of oxide crystals, *J. Crystal Growth,* Vol. 186, 1999, pp. 186–196.

[12]. Z. L. Wang, ZnO nanowire and nanobelt platform for nanotechnology, *Materials Science and Engineering: R,* Vol. 64, 2009, pp. 33–71.

[13]. H. Hu, X. Huang, C. Deng, X. Chen, Y. Qian, Hydrothermal synthesis of ZnO nanowires and nanobelts on a large scale, *Materials Chemistry and Physics,* Vol. 106, 2007, pp. 58–62.

[14]. P. C. Chen, G. Shen, C. Zhou, Chemical sensors and electronic noses based on 1-D metal oxide nanostructures, *IEEE Transactions on Nanotechnology,* Vol. 7, 2008, pp. 668–682.

[15]. S. Wang, Y. Zhao, J. Huang, Y. Wang, S. Wu, S. Zhang, W. Huang, Low-temperature carbon

monoxide gas sensors based gold/tin dioxide, *Solid-State Electron,* Vol. 50, 2006, pp. 1728–1731.
[16]. N. Yamazoe, G. Sakai, K. Shimanoe, Oxide semiconductor gas sensors, *Catalysis Surveys Asia*, Vol. 7, 2003, pp. 63–75.
[17]. S. R. Morrison, Semiconductor gas sensors, *Sensors and Actuators B,* Vol. 2, 1981, pp. 329–341.
[18]. Z. Yang, Y. Huang, G. Chen, Z. Guo, S. Cheng, S. Huang, Ethanol gas sensor based on Al-doped ZnO nanomaterial with many gas diffusing channels. *Sensors and Actuators B,* Vol. 140, 2009, pp. 549–556.
[19]. M. C. Carotta, A. Cervi, V. Natale, S. Gherardi, A. Giberti, V. Guidi, D. Puzzovio, B. Vendemiati, G. Martinelli, M. Sacerdoti, ZnO gas sensors: A comparison between nanoparticles and nanotetrapods-based thick films. *Sensors and Actuators B,* Vol. 137, 2009, pp. 164–169.
[20]. W. Ang, P. Liuhua, H. Wei, Recent progress in the ZnO nanostructure-based sensors, *Materials Science and Engineering B,* Vol. 176, 2011, pp. 1409–1421.
[21]. A. Eunseong, J. Hooncheol, K. Hyojin, K. Dojin, Synthesis and gas sensing properties of ZnO nanostructures, *Journal of the Korean Physical Society,* Vol. 57, 2010, pp. 1784–1788.
[22]. S. K. Lim, S. H. Hwang, S. H. Kim, H. W. Park, Preparation of ZnO nanorods by microemulsion synthesis and their application as a CO gas sensor. *Sensors and Actuators B,* Vol. 160, 2011, pp. 94–98.
[23]. Y. Zeng, L. Qiao, Y. Bing, M. Wen, B. Zou, W. Zheng, Y. Zhang, G. Zou, Development of microstructure CO sensor based on hierarchically porous ZnO nanosheet thin films, *Sensors and Actuators B,* Vol. 05, 2012, pp. 090.
[24]. U. Manzoor, D. K. Kim, Synthesis and enhancement of ultraviolet emission by post-thermal treatment of unique zinc oxide comb-shape dendritic nanostructures, *Scripta Materialia,* Vol. 54, 2006, pp. 807–811.
[25]. M. Amin, N. A. Shah, A. S. Bhatti, M. A. Malik, Effects of Mg doping on optical and CO gas sensing properties of sensitive ZnO nanobelts, *CrystEngComm,* Vol. 6, 2014, pp. 6080-6088.
[26]. R. A. Laudise, A. A. Ballman, *Journal of Physical Chemistry,* Vol. 64, 1960, pp. 688.
[27]. J. Y. Lao, J. Y. Huang, D. Z. Wang, Z. F. Ren, *Nano Letters,* Vol. 3, 2003, pp. 235.
[28]. P. X. Gao, C. S. Lao, Y. Ding, Wang, Z. L., *Advanced Functional Materials,* Vol. 16, 2006, pp. 53.
[29]. Z. Zhang, J. B. Yi, J. Ding, L. M. Wong, H. L. Seng, S. J. Wang, J. G. Tao, G. P. Li, G. Z. Xing, T. C. Sum, C. H. A. Huan, and T. Wu, Cu-Doped ZnO Nanoneedles and Nanonails: Morphological Evolution and Physical Properties, *Journal of Physical Chemistry C,* Vol. 112, Issue 26, 2008, pp. 9579-9585.
[30]. M. Mukhtar, L. Munisa, R. Saleh, Co-Precipitation Synthesis and Characterization of Nanocrystalline Zinc Oxide Particles Doped with Cu^{2+} Ions, *Materials Sciences and Applications,* Vol. 3, 2012, pp. 543-551.
[31]. M. Amin, U. Manzoor, M. Islam, A. S. Bhatti and N. A. Shah, Synthesis of ZnO Nanostructures for Low Temperature CO and UV Sensing. *Sensors,* Vol. 12, 2012, pp. 13842-13851.
[32]. J. A. Reddy, M. K. Kokila, H. Nagabhushana, R. P. S. Chakradhar, C. Shivakumara, J. L. Rao and B. M. Nagabhushana, Structural, Optical and EPR Studies on ZnO:Cu Nanopowders Prepared via Low Temperature Solution Combustion Synthesis, *Journal of Alloys and Compounds,* Vol. 509, Issue 17, 2011, pp. 5349-5355.
[33]. Y. Chen and X. L. Xu, Effect of Oxygen Deficiency on Optical Band Gap Shift in Er-Doped ZnO Thin Films, *Physica B: Condensed Matter,* Vol. 406, Issue 17, 2011, pp. 3121-3124.
[34]. K. G. Kanade, B. B. Kale, J.-O. Baeg, S. M. Lee, C. W. Lee, S.-J. Moon and H. Chang, Self-Assembled Aligned Cu Doped ZnO Nanoparticles for Photocatalytic Hydrogen Production under Visible Light Irradiation, *Materials Chemistry and Physics,* Vol. 102, Issue 1, 2007, pp. 98-104.